Polarity and permeation profiles in lipid membranes

Derek Marsh*

Abteilung Spektroskopie, Max-Planck-Institut für Biophysikalische Chemie, 37070 Göttingen, Germany

Edited by Harden M. McConnell, Stanford University, Stanford, CA, and approved May 1, 2001 (received for review January 16, 2001)

The isotropic ^{14}N-hyperfine coupling constant, a_o^N, of nitroxide spin labels is dependent on the local environmental polarity. The dependence of a_o^N in fluid phospholipid bilayer membranes on the C-atom position, *n*, of the nitroxide in the *sn*-2 chain of a spin-labeled diacyl glycerophospholipid therefore determines the transmembrane polarity profile. The polarity variation in phospholipid membranes, with and without equimolar cholesterol, is characterized by a sigmoidal, trough-like profile of the form $\{1 + \exp[(n - n_o)/\lambda]\}^{-1}$, where $n = n_o$ is the point of maximum gradient, or polarity midpoint, beyond which the free energy of permeation decreases linearly with *n*, on a characteristic length-scale, λ. Integration over this profile yields a corresponding expression for the permeability barrier to polar solutes. For fluid membranes without cholesterol, $n_o \approx 8$ and $\lambda \approx 0.5$–1 CH_2 units, and the permeability barrier introduces an additional diffusive resistance that is equivalent to increasing the effective membrane thickness by 35–80%, depending on the lipid. For membranes containing equimolar cholesterol, $n_o \approx 9$–10, and the total change in polarity is greater than for membranes without cholesterol, increasing the permeability barrier by a factor of 2, whereas the decay length remains similar. The permeation of oxygen into fluid lipid membranes (determined by spin-label relaxation enhancements) displays a profile similar to that of the transmembrane polarity but of opposite sense. For fluid membranes without cholesterol $n_o \approx 8$ and $\lambda \approx 1$ CH_2 units, also for oxygen. The permeation profile for polar paramagnetic ion complexes is closer to a single exponential decay, i.e., n_o lies outside the acyl-chain region of the membrane. These results are relevant not only to the permeation of water and polar solutes into membranes and their permeabilities, but also to depth determinations of site-specifically spin-labeled protein residues by using paramagnetic relaxation agents.

The permeation profiles of water and polar solutes into lipid membranes are fundamental not only to transport studies but also to the energetics of insertion of proteins into membranes. Additionally, the permeation profiles of paramagnetic relaxation agents are of practical importance for depth determinations in membranes by site-directed spin labeling (1). Trough-like polarity profiles across lipid membranes have been established by measuring isotropic ^{14}N-hyperfine splitting constants, a_o^N, or the principal hyperfine tensor element, A_{zz}, in lipid membranes (2–4). These are probably determined to a large extent by the penetration of water into the hydrophobic interior. This will modulate the energetics of burying amino acid residues in membranes, but has largely been neglected in favor of a uniform hydrophobic effect when analyzing the stability of integral membrane proteins (e.g., ref 5). White and Wimley (6) are among the few authors who have addressed this problem specifically. Interestingly, experiments on paramagnetic enhancements of spin labels by molecular oxygen and by paramagnetic ion complexes (7) have suggested that the free energy of permeation (or at least the difference in free energy for these complementary relaxation agents) is a linear function of penetration distance into the membrane. This implies exponential permeation profiles.

In the present communication, I characterize the polarity profiles derived from spin-label measurements with different lipid membranes by using an analytical expression that is sigmoidal and decays exponentially toward to the mid-plane of the membrane. This profile is thermodynamically based, and may be transformed directly into the membrane permeability barrier for polar solutes. The same functional dependence is also useful for characterizing oxygen penetration into membranes and, in a truncated form, for permeation profiles of polar paramagnetic complexes that are commonly used in site-directed spin labeling. Analogies with the fluid membrane diffraction profiles of Wiener and White (8) are persuasive and enlightening.

Materials and Methods

Materials. Phospholipids were from Avanti Polar Lipids and cholesterol was from Merck. Spin-labeled phosphatidylcholines, *n*-PCSLs {1-acyl-2-[*n*-(4,4-dimethyloxazolidine-*N*-oxyl)-stearoyl]-*sn*-glycero-3-phosphocholine}, were synthesized as described in Marsh and Watts (9).

Sample Preparation. Phospholipids with or without 50 mol % cholesterol were dissolved in dichloromethane with 1 mol % of the desired *n*-PCSL ($n = 4, 5, 6, 7, 8, 9, 10, 11, 12, 13, 14$, or 16). After removal of organic solvent and vacuum drying, the lipids were dispersed in 10 mM Tris 0.1 M KCl (pH 8.0) buffer. For unsaturated lipids, samples and buffer were saturated with argon. Hydrated samples were pelleted in 1-mm diameter glass capillaries. These were then accommodated in a standard quartz EPR tube that contained light silicone oil for thermal stability. See ref. 10 for further details.

EPR Spectroscopy. Spectra were recorded on a Varian Century-Line 9-GHz spectrometer at 5° intervals from 25°C to 70°C. Samples were thermostated by nitrogen gas flow. Temperature was measured with a fine-wire thermocouple adjacent to the sample at the top of the cavity. Isotropic ^{14}N-hyperfine constants were determined from the relation:

$$a_o^N = \tfrac{1}{3}(A_\parallel + 2A_\perp), \qquad [1]$$

where $A_\perp$ and $A_\parallel$ are the hyperfine constants determined with the magnetic field perpendicular and parallel, respectively, to the membrane normal. The latter were determined from the outer and inner spectral hyperfine splittings with corrections given in Marsh (11). The anisotropic spectra were recorded at temperatures sufficiently high that the spectral splittings were unaffected by slow motional contributions (10). For spectra of spin labels close to the terminal methyl group of the lipid chains, the spectral anisotropy is small and not well resolved. In these cases, a temperature sufficiently high to give totally isotropic spectra was used so that the spectral hyperfine splittings are equal to a_o^N itself. For both the former and latter cases, the experimental criterion for validity is that the (effective) values derived for a_o^N should have little or no temperature dependence. Typically, measurements from 5–10 spectra recorded at 5°C intervals in

This paper was submitted directly (Track II) to the PNAS office.

Abbreviations: *n*-PCSL, spin-labeled phosphatidylcholines having the structure 1-acyl-2-[*n*-(4,4-dimethyloxazolidine-*N*-oxyl)stearoyl]-*sn*-glycero-3-phosphocholine; *n*-SASL, *n*-(4,4-dimethyloxazolidine-*N*-oxyl)stearic acid; DPPC, 1,2-dipalmitoyl-*sn*-glycero-3-phosphocholine; DMPC, 1,2-dimyristoyl-*sn*-glycero-3-phosphocholine; DOPC, 1,2-dioleoyl-*sn*-glycero-3-phosphocholine; POPC, 1-palmitoyl-2-oleoyl-*sn*-glycero-3-phosphocholine.

*E-mail: dmarsh@gwdg.de.

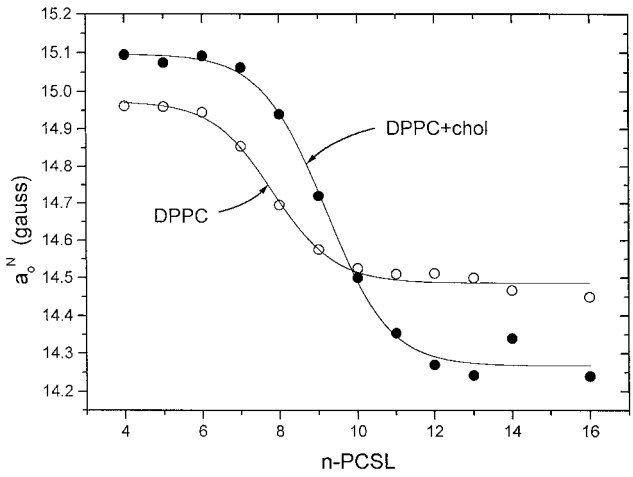

Fig. 1. Polarity profiles of the isotropic ^{14}N-hyperfine coupling constant, a_o^N, of *n*-PCSL spin labels in fluid bilayer membranes of dipalmitoyl phosphatidylcholine (DPPC) (○) and of DPPC plus 50 mol % cholesterol (●). Data are from ref. 4 and additional measurements. Errors in mean a_o values are in the range ± 0.05–0.15 G. Lines represent nonlinear least-squares fits with Eq. **2**. The fitting parameters and uncertainties are given in Table 1.

this range were averaged. Errors in the mean value were 0.05–0.1 G, or less, depending on lipid and spin-label position. Measurements used were confined to a single fluid or liquid-ordered phase, and there was no hint of any pronounced spin-spin broadening in the spectra that might indicate inhomogeneities in probe distribution.

Results

Polarity Profiles from Spin Labels. Values of the isotropic hyperfine coupling constant, a_o^N, of spin-labeled glycerophospholipids with the nitroxide group at position *n* in the *sn*-2 chain (*n*-PCSL) were obtained from the EPR spectra of the *n*-PCSLs at probe amounts in fluid phospholipid bilayer membranes as described in *Materials and Methods* (see also refs. 11 and 12). A typical transmembrane profile of the isotropic hyperfine splitting constants is given in Fig. 1 for *n*-PCSL in fluid dipalmitoyl phosphatidylcholine (DPPC) membranes. The profile for liquid-ordered DPPC membranes that contain equimolar cholesterol is also shown in the same figure. There are very significant differences between the polarity profiles of DPPC membranes with and without cholesterol. Nevertheless, both profiles have the same overall trough-like shape. Corresponding data were obtained for dimyristoyl phosphatidylcholine (DMPC) membranes and for 1-palmitoyl-2-oleoyl and dioleoyl phosphatidylcholine (POPC and DOPC) membranes, with and without equimolar cholesterol. These lipids also produced trough-like profiles in the fluid phase, with qualitatively similar modifications by cholesterol, but with significant differences between saturated and unsaturated lipids (see below).

Fitting the Polarity Profiles. The trough-like dependence of the isotropic ^{14}N-hyperfine-coupling constant, a_o^N, on spin-label position, *n*, in the lipid chain (Fig. 1) is of the following form:

$$a_o^N(n) = \frac{a_{o,1}^N - a_{o,2}^N}{1 + e^{(n - n_o)/\lambda}} + a_{o,2}^N, \qquad [2]$$

where $a_{o,1}^N$ and $a_{o,1}^N$ are the limiting values of a_o^N at the polar headgroup and terminal methyl ends of the chain, respectively, and λ is an exponential decay constant. Eq. **2** applies to all *n*, and n_o is the value of *n* at the point of maximum gradient, corresponding to $a_o^N(n_o) = \frac{1}{2}(a_{o,1}^N + a_{o,2}^N)$. For large *n*, the dependence becomes a simple exponential. The profile given by Eq. **2** is exactly antisymmetric about the position n_o. A physically plausible asymmetry could be introduced, requiring a further adjustable parameter. To within the sensitivity of the data, however, this refinement is not justified.

Eq. **2** corresponds to the so-called Boltzmann sigmoidal form, and has a relatively straightforward thermodynamic interpretation. It corresponds to a normalized two-phase distribution, $\approx\exp[-(n - n_o)/\lambda]$, between outer and inner regions of the membrane that are defined by $n < n_o$ and $n > n_o$, respectively. The free energy of transfer, $(n - n_o)k_BT/\lambda$, increases linearly with the distance, $n - n_o$, into the inner region. It seems intuitively reasonable to identify these two membrane regions with the interfacial region and hydrocarbon core, respectively, that were defined by Wiener and White (8) by using diffraction methods. A quantitative comparison with the latter results is given later.

The fitted curves in Fig. 1 demonstrate that Eq. **2** provides an adequate description of the polarity profiles for fluid phospholipid membranes both in the presence and in the absence of cholesterol. The parameters determined by nonlinear least-squares fitting are given in Table 1, which includes data from all lipid bilayer membranes studied. Data are also given for bovine chromaffin granule membranes and bilayers of their extracted

Table 1. Parameters fitting the polarity profile of the isotropic ^{14}N-hyperfine coupling of *n*-PCSL or *n*-SASL spin labels in different lipid membranes, according to Eq. 2

Lipid	$a_{o,1}^N$, G	$a_{o,2}^N$, G	n_o	λ
DPPC	14.97 ± 0.02	14.49 ± 0.01	7.8 ± 0.1	0.8 ± 0.1
DPPC + chol	15.10 ± 0.02	14.27 ± 0.02	9.2 ± 0.1	0.8 ± 0.1
DMPC	15.03 ± 0.01	14.40 ± 0.01	8.00 ± 0.06	0.44 ± 0.06
DMPC + chol	15.11 ± 0.02	14.25 ± 0.02	9.37 ± 0.09	0.83 ± 0.08
POPC	15.22 ± 0.03	14.46 ± 0.02	8.35 ± 0.14	1.03 ± 0.13
POPC + chol	15.31 ± 0.03	14.23 ± 0.03	9.38 ± 0.14	1.25 ± 0.13
DOPC	15.27 ± 0.04	14.55 ± 0.03	8.24 ± 0.24	0.96 ± 0.22
DOPC + chol	15.27 ± 0.02	14.33 ± 0.03	10.0 ± 0.1	1.0 ± 0.1
CG lipid	15.15 ± 0.04	14.10 ± 0.04	9.5 ± 0.2	0.5 ± 0.2
CG membrane	15.15 ± 0.04	14.00 ± 0.04	9.5 ± 0.2	0.8 ± 0.2

Measurements are with *n*-PCSL, except for chromaffin granule (CG) lipids and membranes, which are with the corresponding spin-labeled stearic acids, *n*-SASL [*n*-(4,4-dimethyloxazolidine-*N*-oxyl)stearic acid]. Data for DPPC ± cholesterol (chol) are from ref. 4 with additional measurements; for DMPC data are from ref. 13, and for CG lipids and membranes data are from ref. 14. Twelve independent values of *n* are used for the fits, except for DMPC ± cholesterol (11 values) and CG membranes and lipids (6 values).

Table 2. Effective water permeation indices, p_1 and p_2, at the polar–apolar interface and center of the membrane, respectively

Lipid	Spin label	p_1	p_2	Δp*
DPPC	*n*-PCSL	0.39 ± 0.02	0.24 ± 0.01	0.15 ± 0.03
DPPC + chol	*n*-PCSL	0.50 ± 0.02	0.11 ± 0.01	0.39 ± 0.03
DMPC	*n*-PCSL	0.44 ± 0.01	0.19 ± 0.01	0.25 ± 0.02
DMPC + chol	*n*-PCSL	0.51 ± 0.02	0.09 ± 0.01	0.42 ± 0.03
POPC	*n*-PCSL	0.60 ± 0.02	0.23 ± 0.01	0.37 ± 0.03
POPC + chol	*n*-PCSL	0.68 ± 0.02	0.08 ± 0.02	0.60 ± 0.04
DOPC	*n*-PCSL	0.64 ± 0.03	0.28 ± 0.02	0.36 ± 0.05
DOPC + chol	*n*-PCSL	0.64 ± 0.02	0.14 ± 0.02	0.51 ± 0.04
CG lipid	*n*-SASL	0.54 ± 0.03	0.0 ± 0.03	0.54 ± 0.06
CG membrane	*n*-SASL	0.54 ± 0.03	−0.06 ± 0.03	0.60 ± 0.06

Values are calculated from the data of Table 1, according to Eq. **3**, and are normalized to the (polarity-corrected) difference in a_o^N between pure water and hydrocarbon, as described in the text.
*$\Delta p = p_1 - p_2$.

lipids derived from measurements with spin-labeled stearic acid, *n*-SASL [*n*-(4,4-dimethyloxazolidine-*N*-oxyl)stearic acid].

The parameters for both DMPC and DPPC membranes without cholesterol are rather similar, particularly with regard to the limiting values ($a_{o,1}^N$ and $a_{o,2}^N$) and the values of n_o (≈8) that characterize the steepest part of the polarity profile (Table 1). The 9–10-*cis* unsaturated bond of the oleoyl chain in POPC and DOPC modifies the profile somewhat, relative to that of DPPC bilayers with fully saturated chains. The midpoint position of the profile ($n_o \approx 8$) is similar, but the width of the transition region ($\lambda = 1.0$) is significantly broadened. (In contrast, the lower order of unsaturated lipid bilayers would tend to increase the effective values of both n_o and λ when expressed in terms of chain segment position.) In addition, the polarity in regions closer to the membrane surface is higher for the unsaturated lipids. The large difference in polarity reported between saturated and unsaturated lipids in the central region of frozen membranes (3) is not found, however, for fluid membranes.

In membranes that contain equimolar cholesterol, which includes chromaffin granule membranes and their extracted lipids, the point of steepest slope is shifted away from the membrane surface to $n_o \approx 9$–10 CH_2 units. Concomitantly, the total extent of the profile is increased to higher polarities closer to the membrane surface, and lower polarities at the membrane mid-plane. These consistent changes are undoubtedly associated with the well-known ordering effect of cholesterol on fluid lipid chains, in addition to a spacing function at the polar headgroup region of the lipids. Qualitatively similar effects of cholesterol have been observed previously on the polarity profiles in frozen membranes (3).

Discussion

A consistent interpretation of the transmembrane polarity profile sensed by systematically spin-labeled lipid positional isomers is possible in terms of the physically realistic model that is represented by Eq. **2**. Cholesterol very markedly modifies this profile, the consequences of which will be seen below. In the following discussion, the polarity profile is related to water permeation and permeability, to the permeation profiles of apolar and polar solutes, and to structural measurements. Finally, the application to site-directed spin-labeling with paramagnetic relaxation agents is considered.

Water Permeation. The polarity profile registered by the spin-label isotropic hyperfine splitting constants can, at least in part, be related to water penetration into the lipid membranes. Experiments in aprotic solvents with increasing concentrations of H-bond donor (15) have revealed a linear dependence of a_o^N on increasing concentration of water, after allowance for changes in dielectric constant. The complete polarity dependence of the isotropic ^{14}N-hyperfine coupling constant can be expressed as follows (see, for example, refs. 12 and 15):

$$a_o^N = K_v(\varepsilon - 1)/(\varepsilon + 1) + a_o^{\varepsilon=1} + K_h p, \qquad [3]$$

where ε is the local dielectric constant of the medium and p is the local proton donor concentration. The values of the scaling parameter K_v and the limiting value $a_o^{\varepsilon=1}$ depend on the type of nitroxide. For the oxazolidine-*N*-oxyl radicals considered here, $K_v = 0.64$ G and $a_o^{\varepsilon=1} = 13.85 \pm 0.09$ G (12). The polarity profiles parametrized in Table 1 can be related to membrane permeation profiles for water molecules by means of the last term on the right in Eq. **3**. In the absence of H-bonding (i.e., $p = 0$) the isotropic hyperfine constants predicted from Eq. **3** are $a_o^{\varepsilon=80} = 14.5$ G and $a_o^{\varepsilon=2} = 14.1$ G in media with dielectric constants $\varepsilon = 80$ (water) and $\varepsilon = 2$ (hydrocarbon), respectively. These polarity-corrected values are used as references to determine the H-bond contribution to $a_{o,1}^N$ and $a_{o,2}^N$, respectively, in the outer and inner regions of the membrane. The part of the polarity profile attributed to water penetration is then expressed in terms of the fractional increment relative to pure water, for which $a_o = 15.7$ G. The corresponding values of water penetration, p_1 and p_2, that refer to the extremes of the a_o^N-profile are given in Table 2. It should be emphasized that these effective values depend on the limiting assumptions that have been made for the local dielectric constant, which is difficult to estimate reliably. They are, however, in some sense a measure for the local water activity that must be in equilibrium with that of the unlabeled lipid environment.

Membrane Permeabilities. It is seen from Table 2 that, in the presence of 50 mol % cholesterol, relatively little water is present at the center of the membrane, whereas as in fluid bilayer membranes without cholesterol an appreciable amount of water permeates to the mid-plane of the membrane. This result correlates with the reduced water permeability of lipid membranes that contain cholesterol (16, 17). At the polar headgroup end of the hydrophobic region of the membrane, the extent of water permeation is considerably higher for unsaturated lipids, as seen by the substantially increased values of p_1.

The permeability coefficient, P, of a membrane to polar solutes is related to the transmembrane polarity or permeation profile by Diamond and Katz (18).

$$1/P = 1/k' + 1/k'' + \int_o^{2d} \frac{dx}{K(x)D(x)}, \qquad [4]$$

BIOPHYSICS

where k' and k'' are the rate constants for solute entry at the two faces of the membrane and $2d$ is the membrane thickness of the hydrophobic region. The permeability barrier of the latter is given by the integral in Eq. **4**, where $K(x)$ and $D(x)$ are the local partition coefficient and diffusion coefficient, respectively, of the solute at distance x into the membrane. From Eq. **3**, it is reasonable to assume that the product $K(x)D(x)$ has a transmembrane profile of the form given in Eq. **2**. The value of $K(x)$ is proportional to the local water concentration, p, and that of K_h in Eq. **3** will depend on the local diffusion-controlled on-rate, specified by $D(x)$ (see ref. 15). For the case of oxygen and paramagnetic complexes, considered later, the accessibilities measured from spin-label relaxation enhancements are explicitly proportional to the $K(x)D(x)$, concentration-diffusion product (19).

Performing the integration in Eq. **4** by using the profile given by Eq. **2**, yields the following contribution, $\delta(1/P)$, to the permeability barrier.

$$\delta(1/P) = \frac{2}{K_1D_1}\left[d + \lambda\left(\frac{K_1D_1}{K_2D_2} - 1\right) \times \ln\left(\frac{K_1D_1/K_2D_2 + e^{(d-d_o)/\lambda}}{K_1D_1/K_2D_2 + e^{-d_o/\lambda}}\right)\right], \qquad [5]$$

where d_o is the distance corresponding to chain position n_o, and λ is also expressed as a distance. K_1D_1 and K_2D_2 are the partition coefficient and diffusion coefficient products at the beginning of the apolar region and at the center of the membrane, respectively. The first term in square brackets on the right side of Eq. **5** represents the normal diffusive resistance of a uniform membrane of thickness $2d$ that is characterized by a partition coefficient K_1 and a diffusion coefficient D_1. The remaining term represents the additional resistance contributed by the permeability barrier. From the spin-label results, the ratio K_1D_1/K_2D_2 can be approximated by the values of p_1/p_2 from Table 2. Together with the data of Table 1, the effective increase in membrane thickness by the permeability barrier that is predicted by the second term on the right of Eq. **5** corresponds to ≈12 (28) CH_2 units for DPPC (POPC) membranes. This value is effectively increased by a further 38 (54) CH_2 units on admixture of equimolar cholesterol. A value of d corresponding to 17 (17.6) CH_2 units (including terminal methyl contacts) was used for these estimates. The ratio of permeabilities with and without cholesterol is then predicted to be 0.54 in both cases, assuming that the barrier given by Eq. **5** is rate limiting. This prediction is in reasonable agreement with experiments on water permeability, which is reduced by ≈50% on addition of equimolar cholesterol (16, 20). Finally, an order of magnitude estimate of the size of the permeability barrier to water can be made taking values of $K_1 = 6.4 \times 10^{-5}$ and $D_1 = 5 \times 10^{-5}$ cm^2·s^{-1} from measurements on water partitioning into hexadecane (21, 22). With an average increment of ≈0.1 nm per methylene group (23), this yields a value of $P \approx 5\text{–}7 \times 10^{-3}$ cm·s^{-1}, which is of comparable size to the water permeabilities found experimentally (20, 24, 25).

Profiles for Oxygen and Polar Ion Complexes. Water permeation profiles might be expected to be mirrored by those of other small polar solutes. In fact, the permeation profile of apolar molecular oxygen, which is preferentially concentrated in the hydrophobic interior of lipid membranes, is also remarkably similar to the polarity profiles presented in Fig. 1 (19). The permeation profile understandably has the opposite sense, however, to that for the polarity or permeation of water. The oxygen permeation profile determined by the paramagnetic relaxation enhancement of spin-labeled phospholipids (see ref. 26) is given in Fig. 2. This may be well fitted by an expression analogous to Eq. **2** with $a^N_{o,2}$>

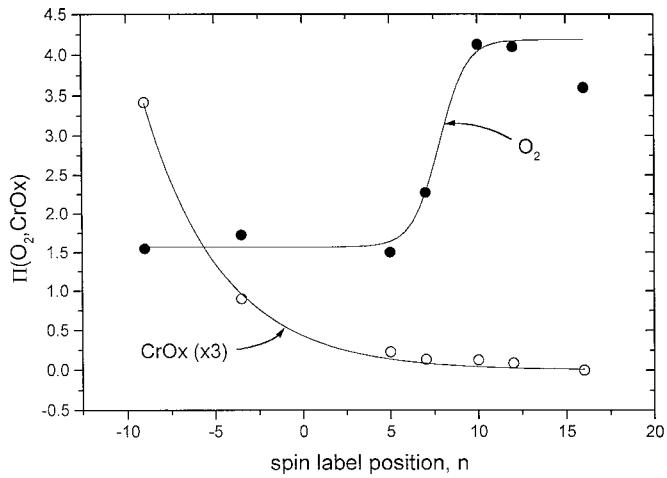

Fig. 2. Permeation profiles, Π, for oxygen (O_2, ●) and chromium oxalate (CrOx, ○) deduced from spin-lattice relaxation enhancements of *n*-PCSL spin labels in rod outer segment disk membranes (data from ref. 26). For CrOx, the values are scaled by a factor of 3. Solid line for O_2 represents a nonlinear least squares fit with an expression equivalent to Eq. **2**. Fitting parameters are: $n_o = 7.8 \pm 0.2$, with the decay constant fixed at $\lambda = 0.78$. Solid line for CrOx is a simple exponential decay, starting at $n = -9$ with a decay constant $\lambda = 4.35 \pm 0.24$. The spin labels positioned at $n = -3.5$ and $n = -9$ represent *N*-TEMPO-stearamide and *N*-TEMPO-phosphatidylcholine (TEMPO is 2,2,6,6-tetramethylpiperidine-*N*-oxyl) , respectively, with the nitroxide in the polar headgroup region of the lipid molecule.

$a^N_{o,1}$. Significantly, the value obtained for n_o (≈7.8) is that characteristic of cholesterol-free membranes determined above from the polarity profile characterized by the spin-label isotropic hyperfine splitting, a^N_o (cf. Fig. 1). The extension into the lipid headgroup region of the fit in Fig. 2 is justified only to within the relatively limited amount of data available in this region. Polarity profiles from frozen membranes of unsaturated lipids (3) tend also to support such an extrapolation.

In contrast, the permeation profiles for polar paramagnetic ion complexes differ significantly from those for the polarity profiles that are given in Fig. 1. For chromium oxalate (Fig. 2), the permeation profile determined by paramagnetic relaxation enhancement of the spin-labeled lipids is better approximated by a simple exponential dependence. (See also data for nickel acetyl acetonate in ref. 7.) This positional dependence corresponds to that described by Eq. **2** for $n_o \ll n$, i.e., in this case, the transition point determined by n_o lies outside the hydrophobic region of the membrane. It therefore follows that, in the case of polar paramagnetic ion complexes, the free energy of membrane permeation has an approximately linear dependence on penetration distance (cf. ref 7).

In general, however, the permeation free energy that corresponds to the concentration profile given by Eqs. **2** and **3**, e.g., for water or oxygen, is not a linear function of the depth of penetration into the membrane. The linearity observed in the logarithm of the ratio of accessibilities to oxygen and paramagnetic complexes (7) therefore must be dominated by the exponential dependence for the paramagnetic complex (Fig. 2). This ratio method has proved extremely useful for determining vertical positions within the membrane, particularly in site-directed spin-labeling. Fitting the profiles for the accessibilities to oxygen and paramagnetic complexes separately, as done here in Fig. 2, has potential for improving the precision of such determinations.

Relation to Transmembrane Dimensions. Up to this point, the representation of the polarity and permeation profiles has been

given in terms of the C-atom position in the phospholipid *sn*-2 acyl chain. In fluid lipid bilayer membranes not containing cholesterol, the mean C–C separation projected onto the membrane normal is ≈0.1 nm per methylene segment (ref. 23). This conversion may be used to express the profiles in terms of transbilayer separations. In fact, the effective spin-label positions $n = -3.5$ and $n = -9$ given in Fig. 2 have been derived in this way from the positions defined in the original work (26). To obtain the entire transbilayer profile, it is necessary to allow for the separation of the terminal methyl groups between the apposing monolayers. From the crystal structure of dilauroyl phosphatidylethanolamine (27), this separation is estimated as ≈0.55 nm, allowing also for the 1.5 CH_2 units offset between the *sn*-1 and *sn*-2 chains. For fluid phospholipid bilayers with C-18 chains, the width of the hydrophobic barrier between the points specified by n_o is then estimated as 2.55 nm. For comparison, the dynamic thickness of the hydrocarbon core of fluid DOPC bilayers, as represented by time-averaged group distributions from diffraction measurements, is given as 2.86 nm (8). This value was determined from samples with relatively low water content. Allowing for the latter will bring the two values into even closer proximity. Correspondingly, the polarity profile mapped out by the spin-labeled lipid chains correlates with the inner section of the partial charge density profile of DOPC bilayers calculated by White and Wimley (6). The latter was obtained from Gaussian group distributions (3 for all CH_2 groups) that were fitted to diffraction data.

It is further noted that the chain region before the principal hydrophobic barrier (i.e., up to $n = n_o$) is confined entirely to the plateau region of the segmental chain order parameters observed by ^2H NMR (28). This means that the shape of the polarity profile will largely be preserved on translating from a chain-position scale (as in Fig. 1) to a transbilayer distance scale. Foreshortening of the distance profile, relative to the chain-position profile, occurs in the inner region, beyond the order-parameter plateau. Here a_o has achieved an almost constant, low value. For the same reason, the increased width in distribution of segment position toward the end of the chain is also unlikely to bias the profile unduly.

Application to Site-Directed Spin Labeling. Measurements of the accessibility to oxygen of spin labels attached to cysteine residues that are systematically stepped throughout the sequence of the first transmembrane segment of the SKC1 K^+-channel from *Streptomyces lividans* (29) provide a good example of the application to site-directed spin-labeling. The accessibilities that are determined from the relaxation enhancement by oxygen of the single spin-labeled cysteine mutants are given in Fig. 3, as a function of residue position in the primary sequence. This transmembrane domain is situated at the periphery of the channel, exposed to lipid. The oxygen accessibilities display an α-helical periodicity between the lipid-facing and the interior-facing residues.

The accessibility maxima in Fig. 3 map out the oxygen concentration profile in the lipid regions immediately surrounding the protein. These have a dependence on residue position that is similar to Eq. **2** for each side of the membrane. Largest oxygen concentration is in the middle of the membrane (residues 34–38) and lowest oxygen concentration at the two interfacial regions (residues 22 and 50). Because all residues are not fully exposed to oxygen, the oxygen profile envelope defined by these measurements (dashed lines in Fig. 3) is relatively coarse-grained. For this reason the approximate profile was first established by fitting Eq. **2** to the local maxima, for each side of the membrane separately. The resulting profiles were then refined by fitting the following expression, which is an extended version of Eq. **2** that allows for the helical periodicity, to all data points:

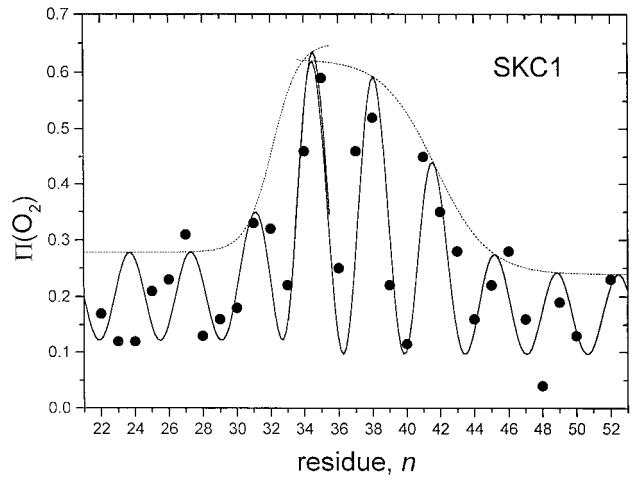

Fig. 3. Oxygen accessibilities, $\Pi(O_2)$, of site-directed spin labels attached to the first transmembrane segment of the SKC1 K^+-channel. Experimental values (29) are given by ●, as a function of the labeled residue position in systematic cysteine-substitution mutants. Dashed lines give the envelope of the oxygen permeation profile at the position of the lipid-facing residues, according to Eq. **2**. Solid lines are the complete oxygen concentration profiles, modulated by the helical residue periodicity of exposure, according to Eq. **6**. The two halves of the membrane, residues 22–36 and 36–50, respectively, are fitted separately as described in the text.

$$\Pi(O_2) = \frac{1}{2}\left[\frac{\Pi_1 - \Pi_2}{1 + \exp\left(\frac{n - n_o}{\lambda}\right)} + \Pi_2\right]\left[1 - \sin\left(\frac{2\pi n}{3.6} + \delta_o\right)\right] + \Pi_o, \quad [6]$$

where the sinusoidal term represents the α-helical periodicity of 3.6 residues per turn, with a phase offset δ_o, and the constant Π_o is the oxygen accessibility of the inward-facing residues. The solid lines in Fig. 3 give the fits to Eq. **6**. For the N-terminal side of the membrane (residues 22–38) the fitting parameters of interest are $n_o = 32.1 \pm 1.2$ and $\lambda = 0.77 \pm 0.75$ residues. For the C-terminal side of the membrane (residues 34–52), the corresponding values are: $n_o = 41.8 \pm 1.2$ and $\lambda = 1.5 \pm 1.1$ residues. It is seen from Fig. 3 that the region of overlap (residues 34–38) between the two halves of the membrane matches reasonably well for the two independent fits.

Comparison can be made with the measurements on lipid bilayer membranes alone, using spin-labeled lipids. The distance between midpoints of the oxygen profile that are specified by n_o is 9.6 ± 2.4 residues. The corresponding distance estimated above for a lipid bilayer with C-16 chains is 2.0–2.2 nm. The rise per residue of an α-helix is 0.15 nm, and the helices in SKC1 are known to be tilted, thus the maximal separation in the latter case is 1.44 ± 0.36 nm. Therefore the width of the oxygen profile at the lipid–protein interface of SKC1 appears significantly narrower than that in lipid bilayer membranes. Part of this difference might be attributable to foreshortening of the lipid chains toward the terminal methyl group. However, part is undoubtedly attributable also to the nonvanishing polarity of the transmembrane protein segments.

The values of the decay length λ, unfortunately, are not determined with great precision because of the coarse-graining that is associated with the α-helical modulation of the accessibilities. They correspond to values of $\lambda = 0.12 \pm 0.11$ and 0.23 ± 0.17 nm for the N- and C-terminal faces of the membrane, assuming a rise of 0.15 nm per residue of an α-helix. This may be compared with values of ≈0.08–0.1 nm obtained for lipid

bilayers by using lipid spin labels (Table 1). At least part of this difference is to be accounted for by the tilting of the helices. A tilt of 46° for the N-terminal section of the helix, and greater for the C-terminal section, would be required to bring the two sets of values into agreement. The tilt of the transmembrane segments determined from the x-ray structure of the SKC1 channel is ≈25° (30). It therefore seems likely that the oxygen profile at the lipid–protein interface is more diffuse than in protein-free bilayers. This result again is in accord with the increase in intramembrane polarity introduced by the transmembrane segments of the protein. For helix D of bacteriorhodopsin, the spread of the oxygen profile appears to be even larger (7).

I thank Frau B. Angerstein for skillful technical assistance.

1. Hubbell, W. L. & Altenbach, C. (1994) in *Membrane Protein Structure: Experimental Approaches.*, ed. White, S. H. (Oxford Univ. Press, New York), pp. 224–248.
2. Griffith, O. H., Dehlinger, P. J. & Van, S. P. (1974) *J. Membr. Biol.* **15,** 159–192.
3. Subczynski, W. K., Wisniewska, A., Yin, J. J., Hyde, J. S. & Kusumi, A. (1994) *Biochemistry* **33,** 7670–7681.
4. Marsh, D. & Watts, A. (1981) in *Liposomes: From Physical Structure to Therapeutic Applications*, ed. Knight, C. G. (Elsevier/North-Holland, Amsterdam), pp. 139–188.
5. Son, H. S. & Sansom, M. S. (1999) *Eur. Biophys. J.* **28,** 489–498.
6. White, S. H. & Wimley, W. C. (1998) *Biochim. Biophys. Acta* **1376,** 339–352.
7. Altenbach, C., Greenhalgh, D. A., Khorana, H. G. & Hubbell, W. L. (1994) *Proc. Natl. Acad. Sci. USA* **91,** 1667–1671.
8. Wiener, M. C. & White, S. H. (1992) *Biophys. J.* **61,** 428–433.
9. Marsh, D. & Watts, A. (1982) in *Lipid-Protein Interactions*, eds. Jost, P. C. & Griffith, O. H. (Wiley-Interscience, New York), Vol. 2, pp. 53–126.
10. Marsh, D. (1982) in *Techniques in Lipid and Membrane Biochemistry,* eds. Metcalfe, J. C. & Hesketh, T. R. (Elsevier, Shannon, Ireland) Vol. B4/II, pp. B426/1–B426/44.
11. Marsh, D. (1985) In *Spectroscopy and the Dynamics of Molecular Biological Systems*, eds. Bayley, P. M. & Dale, R. E. (Academic, London), pp. 209–238.
12. Marsh, D. (1981) in *Membrane Spectroscopy: Molecular Biology, Biochemistry and Biophysics,* ed. Grell, E. (Springer, Berlin), Vol. 31, pp. 51–142.
13. Epperlein, D. (1984) Diploma thesis (Universität Göttingen, Göttingen, Germany).
14. Fretten, P., Morris, S. J., Watts, A. & Marsh, D. (1980) *Biochim. Biophys. Acta* **598,** 247–259.
15. Gagua, A. V., Malenkov, G. G. & Timofeev, V. P. (1978) *Chem. Phys. Lett.* **56,** 470–473.
16. Bittman, R. & Blau, L. (1972) *Biochemistry* **11,** 4831–4839.
17. Schuler, I. S., Milon, A., Nakatani, Y., Ourissen, G., Albrecht, A. M., Benveniste, P. & Hartmann, M. A. (1991) *Proc. Natl. Acad. Sci. USA* **88,** 6926–6930.
18. Diamond, J. M. & Katz, Y. (1974) *J. Membr. Biol.* **17,** 121–154.
19. Subczynski, W. K., Hyde, J. S. & Kusumi, A. (1989) *Proc. Natl. Acad. Sci. USA* **86,** 4474–4478.
20. Finkelstein, A. & Cass, A. (1968) *J. Gen. Physiol.* **52,** 145S–172S.
21. Schatzberg, P. (1963) *J. Phys. Chem.* **67,** 776–779.
22. Schatzberg, P. (1965) *J. Polym. Sci. Part C* **10,** 87–92.
23. Marsh, D. (1990) *Handbook of Lipid Bilayers* (CRC, Boca Raton, FL).
24. Huster, D., Jin, A. J., Arnold, K. & Gawrisch, K. (1997) *Biophys. J.* **73,** 855–864.
25. Olbrich, K., Rawicz, W., Needham, D. & Evans, E. (2000) *Biophys. J.* **79,** 321–327.
26. Farahbakhsh, Z. T., Altenbach, C. & Hubbell, W. L. (1992) *Photochem. Photobiol.* **56,** 1019–1033.
27. Hitchcock, P. B., Mason, R., Thomas, K. M. & Shipley, G. G. (1974) *Proc. Natl. Acad. Sci. USA* **71,** 3036–3040.
28. Seelig, J. & Seelig, A. (1980) *Q. Rev. Biophys.* **13,** 19–61.
29. Perozo, E., Marien Cortes, D. & Cuello, L. G. (1998) *Nat. Struc. Biol.* **5,** 459–469.
30. Doyle, D. A., Morais Cabal, J., Pfuetzner, R. A., Kuo, A., Gulbis, J. M., Cohen, S. L., Chait, B. T. & MacKinnon, R. (1998) *Science* **280,** 69–77.